THE JOURNAL OF PHYSICAL CHEMISTRY B

Article

pubs.acs.org/JPCB

Photocycle of Photoactive Yellow Protein in Cell-Mimetic Environments: Molecular Volume Changes and Kinetics

Cheolhee Yang,[†,‡,§] Seong Ok Kim,[†,‡,§] Yonggwan Kim,[†,‡] So Ri Yun,[†,‡] Jungkweon Choi,*[,†,‡] and Hyotcherl Ihee*[,†,‡]

[†]Center for Nanomaterials and Chemical Reactions, Institute for Basic Science, Daejeon 305-701, Republic of Korea

[‡]Department of Chemistry, KAIST, Daejeon 305-701, Republic of Korea

Supporting Information

ABSTRACT: Using various spectroscopic techniques such as UV−visible spectroscopy, circular dichroism spectroscopy, NMR spectroscopy, small-angle X-ray scattering, transient grating, and transient absorption techniques, we investigated how cell-mimetic environments made by crowding influence the photocycle of photoactive yellow protein (PYP) in terms of the molecular volume change and kinetics. Upon addition of molecular crowding agents, the ratio of the diffusion coefficient of the blue-shifted intermediate (pB) to that of the ground species (pG) significantly changes from 0.92 and approaches 1.0. This result indicates that the molecular volume change accompanied by the photocycle of PYP in molecularly crowded environments is much smaller than that which occurs in vitro and that the pB intermediate under crowded environments favors a compact conformation due to the excluded volume effect. The kinetics of the photocycle of PYP in cell-mimetic environments is greatly decelerated by the dehydration, owing to the interaction between the protein and small crowding agents, but is barely affected by the excluded volume effect. The results lead to the inference that the signaling transducer of PYP may not necessarily utilize the conformational change of PYP to sense the signaling state.

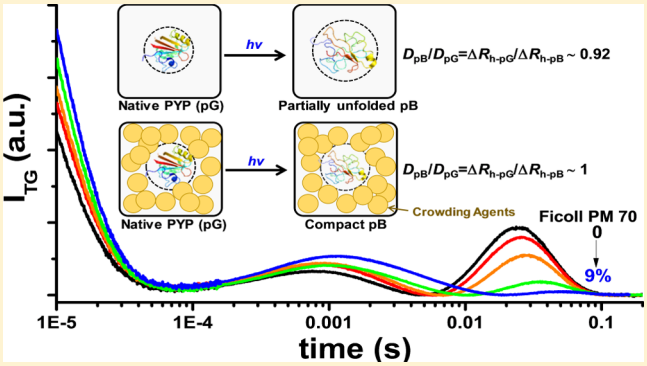

INTRODUCTION

As both the structure and stability of biomolecules are intimately related to their functions within cells, understanding their structure and stability under physiological conditions is of critical importance.[1−3] In this respect, most studies have been performed mainly on various biomolecules in diluted and homogeneous solutions (in vitro), and then their functions in cells are deduced from the results obtained. However, biomolecules in vivo function within crowded intracellular environments containing a number of other highly concentrated species, such as proteins, carbohydrates, lipids, nucleic acids, metabolites, and natural products. In addition, the intracellular environment is very heterogeneous compared to in vitro experimental conditions, in terms of temperature, pH, viscosity, etc. These differences may result in a significant change in the structure and stability of biomolecules.[1,2,4−8]

Generally, the effect induced by the crowded intracellular environment is referred to as the "molecular crowding effect", which has been studied for several decades using chemical agents that can generate a cell-mimetic environment.[1,4,9,10] The molecular crowding effect is manifested as either the excluded volume effect or dehydration effect. The excluded volume effect, which is a nonspecific repulsive interaction between macromolecules, becomes more significant when the structural transition of a biomolecule is accompanied by a considerable volume change and the introduced biomolecule has a comparable size to that of the macromolecules already present. On the other hand, highly crowded environments have an additional effect on the extent of solvation on the surface of biomolecules. Especially, small crowding agents having hydrophilic properties act as osmolytes in aqueous solution, thereby inducing a decrease in the water activity of the system. Consequently, the adsorbed water molecules move away from the surface of biomolecules, resulting in dehydration.

Numerous theoretical and experimental studies have shown that molecular crowding significantly affects biological reactions,[2,8−11] such as protein folding and protein−protein interactions. Nevertheless, the exact effects of molecular crowding remain a controversial issue. In this regard, we used photoactive yellow protein (PYP) as a target protein to explore the effect of molecular crowding on the conformational dynamics of a protein. PYP from *Halorhodospira halophila*, which is a blue-light-sensing protein, has been extensively investigated as a model system for signal transducing proteins.[12−24] Upon irradiation of blue light, PYP undergoes a photocyclic reaction initiated by the photoisomerization of a

Received: December 30, 2016
Revised: January 5, 2017
Published: January 6, 2017

DOI: 10.1021/acs.jpcb.6b13076
J. Phys. Chem. B 2017, 121, 769−779

chromophore, *p*-coumaric acid (*p*CA).[15,20,22] The photocycle of PYP has been explained mainly by two kinetic models: the sequential and parallel models as shown in Figure 1. According

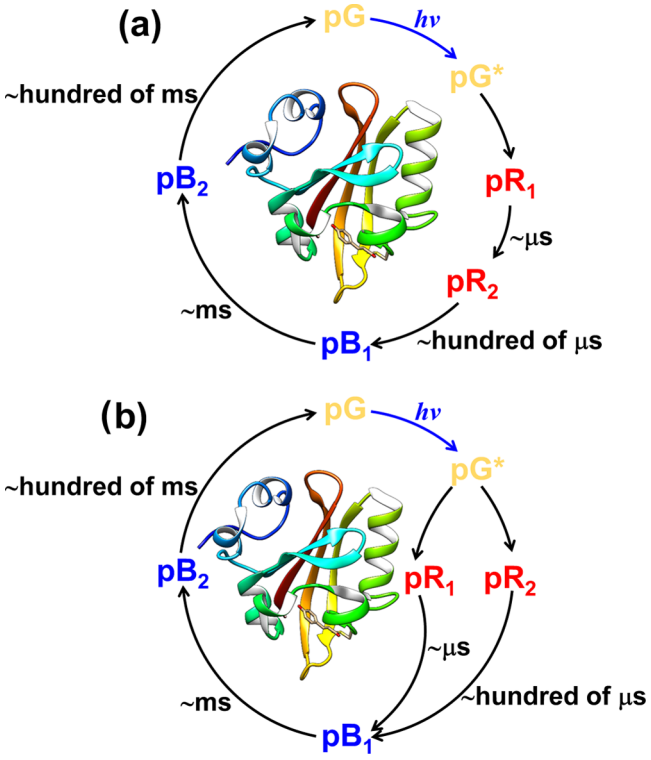

Figure 1. Schematic illustration for the photocycle of PYP: (a) sequential kinetic model and (b) parallel kinetic model. The protein structure is shown in the middle (PDB ID: 2PHY).

to the sequential model,[25−28] the ground-state species, pG, is rapidly converted into a red-shifted intermediate, pR_1, and then transformed to pR_2. The pR_2 species decays on the submillisecond time scale to a blue-shifted intermediate, pB_1. The pB_1 species is converted to the pB_2 species within a few millisecond time scale. Finally, pB_2 returns to pG within a hundred millisecond time scale. In contrast, the parallel model has suggested that pG is rapidly converted to two intermediates, pR_1 and pR_2, and then transformed to pB_1. The pB_1 species is converted to the pB_2 species within a time scale of a few milliseconds. Finally, the pB_2 species returns to the pG state. Regardless of the kinetic model on the photocycle of PYP, the pB_2 species formed during the photocycle of PYP is considered to be involved in the signal transduction process for phototaxis because the formation of pB_2 induces the largest molecular volume change (or conformational change). In this regard, the molecular volume change accompanied by the photocycle of PYP may be a critical determinant in the signal transduction process.

Despite numerous theoretical and experimental studies on the photocycle of PYP, the effect of molecular crowding on the photocycle of PYP still remains as a matter of debate. Although Hellingwerf and co-workers studied the kinetics on the photocycle of PYP in the presence of PEG 2000 and BSA,[15] they did not study the molecular volume change followed by the photocycle of PYP in the molecularly crowded environment. To address this issue, we thoroughly investigated the photocycle of PYP in terms of the molecular volume change and kinetics in a cell-mimetic environment using multiple probes such as the UV−visible (UV−vis) spectroscopy, circular dichroism (CD) spectroscopy, NMR spectroscopy, small-angle X-ray scattering (SAXS), transient grating (TG), and transient absorption (TA) techniques. In this study, ethylene glycol (EG), poly(ethylene glycol) (PEG) 400, PEG 1000, PEG 8000, Ficoll PM 70, Dextran 40, and bovine serum albumin (BSA) were used as molecular crowding agents to generate a cell-mimetic environment.[8,11] Although EG and PEG with a low molecular weight (MW) are good crowding agents for mimicking the intracellular environment, they can also induce dehydration, owing to the release of protein-binding water molecules. In contrast, PEG with a high MW, Ficoll PM 70, Dextran 40, and BSA have only a pure excluded volume effect for proteins.[2,29−32] The TG technique was utilized to probe the global structural change of a protein on the basis of the change in the diffusion coefficient (D), which is directly related to the size and shape of a chemical species.[28,33−35] The TA technique is used to monitor the local structural change around the chromophore. The results obtained in this study clearly demonstrate that the molecular volume change accompanied by the photocycle of PYP in molecularly crowded environments is significantly influenced by the excluded volume effect, whereas the kinetics of the photocycle of PYP is greatly affected by the dehydration of a protein. Furthermore, the photocycle of PYP in a molecularly crowded environment induces much smaller molecular volume changes than those observed in vitro, indicating that the photocycle of PYP in vivo may induce significantly smaller molecular volume change owing to the molecular crowding effect.

RESULTS AND DISCUSSION

As mentioned above, EG and PEG with a low MW can induce changes in the structure and stability of a protein due to dehydration. Therefore, to characterize the structure of PYP in the presence of the small crowding agent, UV−vis absorption, CD, $^1H-^{15}N$ HSQC spectra, and SAXS for PYP in 50 mM Tris−HCl buffer solution (pH 7) were measured. As a result, we found that the small molecular crowding agents can induce a change in the size (and/or shape) of PYP but not in its secondary structure (Figure S1). The $^1H-^{15}N$ HSQC spectra, together with SAXS analysis, demonstrate that molecular crowding agents such as EG and PEG interact with residues in loop regions and in the N-terminal region, resulting in the changes in the apparent molecular size of PYP (see Figures S2−S7).

Molecular Volume Change Followed by the Photocycle of PYP. To understand the molecular volume change followed by the photocycle of PYP in molecularly crowded environments, TG signals after photoexcitation of PYP in 50 mM Tris−HCl buffer (pH 7) were measured with varying concentrations of molecular crowding agents. Figure 2 shows the representative TG signals measured from PYP in the buffer as a function of the concentration of PEG 400 and Ficoll PM 70. All TG signals increase quickly within the excitation pulse width, followed by a weak increase at a submicrosecond time scale, and then decay to a certain intensity with rate constant $D_{th}q^2$ (thermal grating). After the decay of the thermal grating signal, the TG signal shows two growth-decay curves and then eventually decays back to the baseline. Furthermore, the features of all TG signals measured in the presence of molecular crowding agents except BSA are very similar (Figures S8 and S9), although the intensities of the TG signals from PYP are altered by the addition of molecular crowding agents. On one

DOI: 10.1021/acs.jpcb.6b13076
J. Phys. Chem. B 2017, 121, 769−779

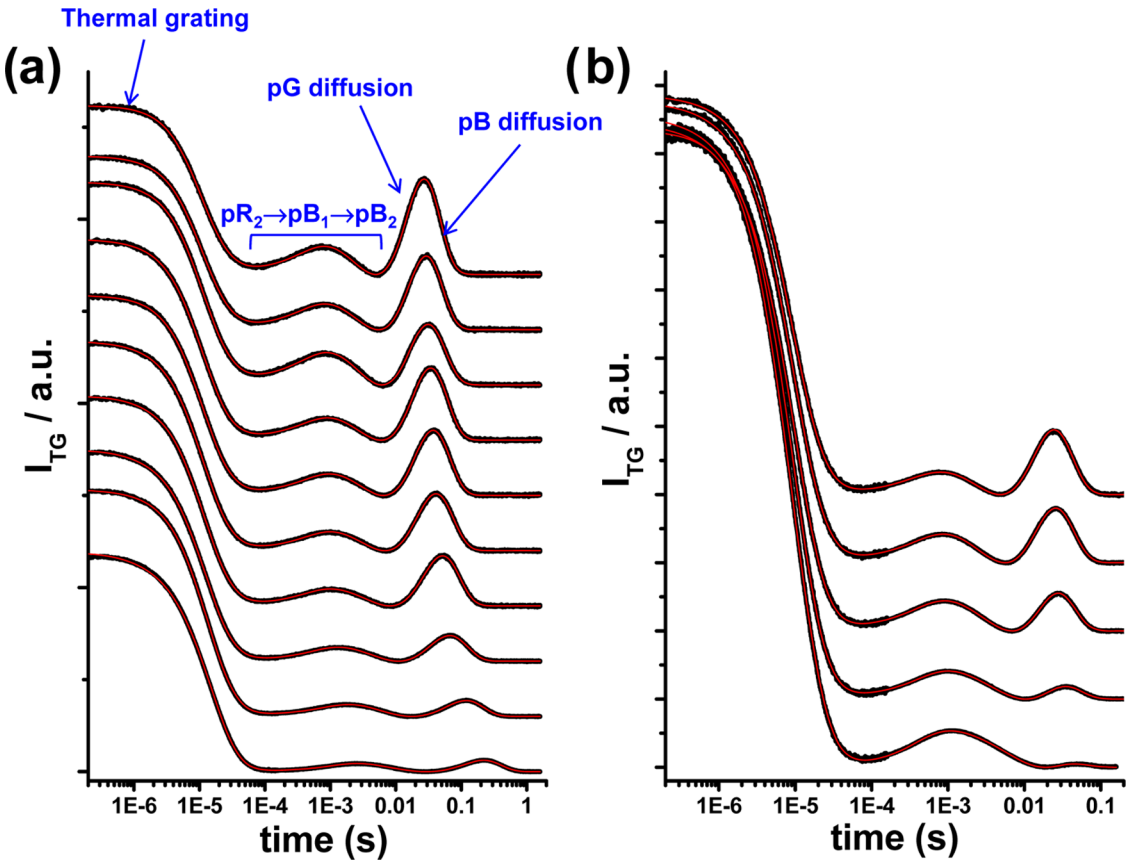

Figure 2. TG signals. TG signals after photoexcitation of PYP as a function of the concentration of PEG 400 (a) and Ficoll PM 70 (b). Experimental signals (black) and theoretical signals (red) calculated by eq 1 are shown. TG signals after photoexcitation of PYP in the presence of PEG 400 and Ficoll PM 70 were measured at $q^2 = 0.40$ and 0.44×10^{12} m^{-2}, respectively. From top to bottom, the concentrations of PEG 400 are 0, 2, 4, 6, 8, 10, 15, 20, 30, and 40% (v/v). From top to bottom, the concentrations of Ficoll PM 70 are 0, 2, 4, 8, and 12% (v/v).

hand, BSA induced significantly different TG signals after photoexcitation of PYP (Figure S10). As shown in Figure S10, TG signals after photoexcitation of PYP in the presence of BSA show a new weak growth-decay curve in the longer time region. This weak TG signal is significantly altered by the change in q^2 value (Figure S10b), indicating that the weak TG signal is attributed to the diffusion processes of chemical species involved in this system, as will be discussed later.

Building on previous studies on the photocyclic reaction of PYP using the TG technique, all TG signals measured in the presence of molecular crowding agents except BSA were fitted using the following function

$$I_{TG} = \left[\delta n_1 \exp\left(-\frac{t}{\tau_1}\right) + \delta n_{th} \exp(-D_{th} q^2 t) + \delta n_2 \exp\left(-\frac{t}{\tau_2}\right) + \delta n_3 \exp\left(-\frac{t}{\tau_3}\right) - \delta n_{pG} \exp(-D_{pG} q^2 t) + \delta n_{pB} \exp(-D_{pB} q^2 t) \right]^2 \quad (1)$$

where δn_1, δn_2, δn_3, δn_{th}, δn_{pG}, and δn_{pB} are the refractive index changes corresponding to exponential decays; τ_1, τ_2, and τ_3 are time constants of photoreactions; D_{th} represents the thermal diffusivity of the solvent; and D_{pG} and D_{pB} are the diffusion coefficients of the pG and pB states of PYP, respectively. The three time constants; τ_1, τ_2, and τ_3; are assigned to the decay of pR_1, the $pR_2 \rightarrow pB_1$ transition, and the $pB_1 \rightarrow pB_2$ transition, respectively. All TG signals observed at various q^2 values in the presence of molecular crowding agents are well-reproduced by eq 1, as shown in Figures 2 and S8, and the determined time constants are summarized in Tables S1. A quantitative analysis of TG signals of PYP in the presence of molecular crowding agents shows that the kinetics on the photocycle of PYP is significantly influenced by the dehydration, owing to the release of protein-binding water molecules rather than the excluded volume effect. The kinetics on the photocycle of PYP in cell-mimetic environments will be discussed in the section Kinetics on the Photocycle of PYP.

Using eq 1, the diffusion coefficients of pG and pB were determined by quantitatively analyzing the TG signals. In the absence of molecular crowding agents, the values of D_{pG} and D_{pB} are 1.18×10^{-10} and 1.08×10^{-10} m^2 s^{-1}, respectively. The D_{pB}/D_{pG} ratio is 0.92, which is consistent with the value reported by Terazima and co-workers.[26] It is known that compared to the D_{pG} value the small D_{pB} value in the absence of molecular crowding agents is attributed to the partially unfolded structure of pB, which is an intermediate formed upon illumination.[26,36] Khan et al. suggested that the unfolded structure of pB mainly arises from the unfolding of the α-helices in the N-terminal region, leading to a change in the hydrogen-bonding pattern between the protein and the aqueous solvent.[26] In a study using a combination of probes; double electron−electron resonance (DEER) spectroscopy, NMR spectroscopy, and time-resolved X-ray solution scatter-

DOI: 10.1021/acs.jpcb.6b13076
J. Phys. Chem. B 2017, 121, 769−779

Table 1. Fitting Results of TG Signals[a]

	with EG					with PEG 400					with PEG 8000				
% (v/v)	D_{pG}	D_{pB}	D_{pB}/D_{pG}	Δf	ΔR_h	D_{pG}	D_{pB}	D_{pB}/D_{pG}	Δf	ΔR_h	D_{pG}	D_{pB}	D_{pB}/D_{pG}	Δf	ΔR_h
0	1.29	1.17	0.91	3.27	1.68	1.16	1.07	0.92	2.98	1.68	1.24	1.13	0.91	3.23	1.68
2 (2.33)[b]	1.23	1.11	0.90	3.61	1.83	1.08	1.00	0.93	3.05	1.61	1.01	0.94	0.93	3.03	1.11
4 (4.65)	1.15	1.06	0.92	3.04	1.46	0.906	0.853	0.94	2.82	1.46	0.823	0.772	0.94	3.30	0.94
6 (6.96)	1.10	1.01	0.92	3.33	1.53	0.860	0.812	0.94	2.83	1.42	0.686	0.649	0.95	3.42	0.77
8 (9.24)	1.06	0.976	0.92	3.34	1.46	0.783	0.742	0.95	2.90	1.40	0.485	0.468	0.96	3.08	0.54
10 (11.5)	0.996	0.925	0.93	3.17	1.32	0.672	0.643	0.96	2.76	1.26	0.425	0.407	0.96	4.28	0.59
15 (17.1)	0.874	0.818	0.94	3.22	1.18	0.554	0.533	0.96	2.92	1.10	0.270	0.26	0.96	5.86	0.45
20 (22.7)	0.767	0.724	0.94	3.18	1.03	0.417	0.404	0.97	3.17	0.92	0.175	0.171	0.98	5.50	0.24
30 (28.1)	0.584	0.559	0.96	3.15	0.79	0.239	0.234	0.98	3.68	0.58	0.119	0.117	0.98	5.91	0.14
40	0.444	0.429	0.97	3.24	0.62	0.128	0.126	0.98	5.10	0.42					

[a] D_{pG} (10^{-10} m^2 s^{-1}) and D_{pB} (10^{-10} m^2 s^{-1}) values in the presence of EG, PEG 400, and PEG 8000. All D_{pG} (10^{-10} m^2 s^{-1}) and D_{pB} (10^{-10} m^2 s^{-1}) values were determined from the global fitting of TG signals using eq 1. The change in friction (Δf, 10^{-12} kg s^{-1}) is calculated using the difference between D_{pG} and D_{pB}. The ΔR_h ($R_{h\text{-}pB} - R_{h\text{-}pG}$, Å) values are determined by eq 3. [b] Values in parentheses indicate the % (v/v) of PEG 8000.

Table 2. Fitting Results of TG Signals[a,b]

	with Ficoll PM 70					with Dextran 40				
% (v/v)	D_{pG}	D_{pB}	D_{pB}/D_{pG}	Δf	ΔR_h	D_{pG}	D_{pB}	D_{pB}/D_{pG}	Δf	ΔR_h
0	1.21	1.10	0.91	3.40	1.80	1.27	1.17	0.92	2.77	1.47
1 (2)	1.18	1.08	0.92	3.23	1.60	1.30	1.20	0.92	2.64	0.94
3 (4)	1.19	1.12	0.94	2.16	0.90	1.09	1.02	0.94	2.59	0.58
6	0.96	0.91	0.95	2.35	0.57					
9	0.84	0.82	0.98	1.19	0.16	0.85	0.82	0.96	1.77	0.16

[a] D_{pG} (10^{-10} m^2 s^{-1}) and D_{pB} (10^{-10} m^2 s^{-1}) values in the presence of Ficoll PM 70 and Dextran 40. All D_{pG} (10^{-10} m^2 s^{-1}) and D_{pB} (10^{-10} m^2 s^{-1}) values were determined from the global fitting of TG signals using eq 1. The change in friction (Δf, 10^{-12} kg s^{-1}) is calculated using the difference between D_{pG} and D_{pB}. The ΔR_h ($R_{h\text{-}pB} - R_{h\text{-}pG}$, Å) values are determined by eq 3. [b] Values in parentheses indicate the % (v/v) of Dextran 40.

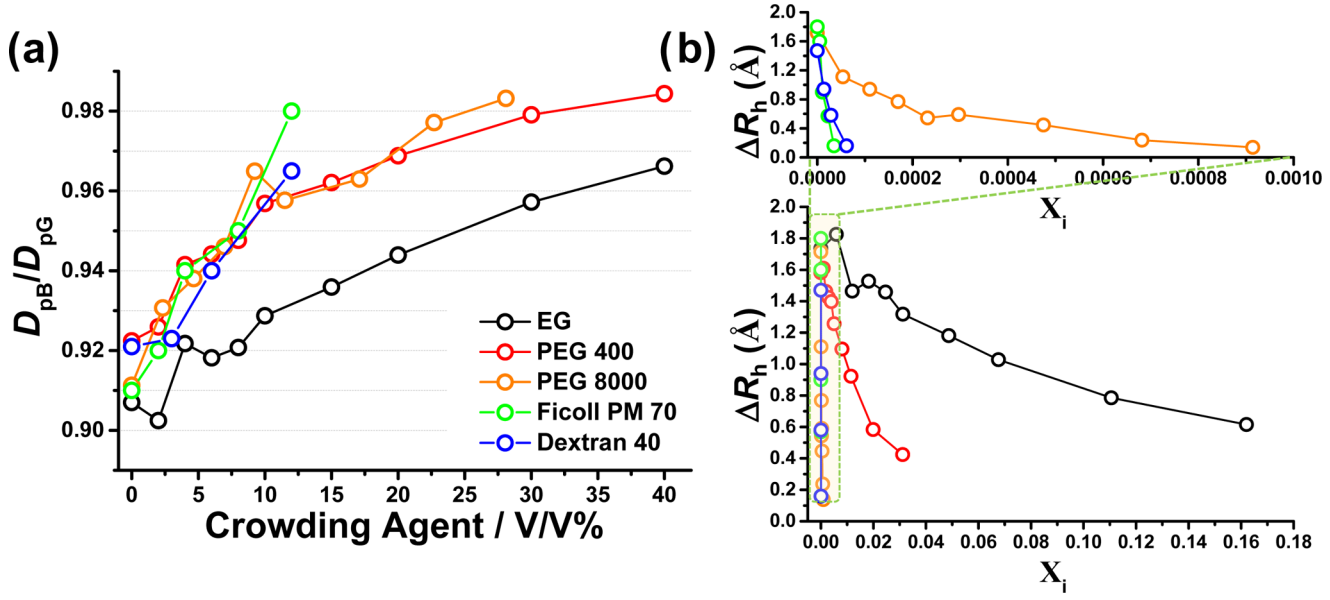

Figure 3. Changes in D_{pB}/D_{pG} ratios upon addition of molecular crowding agents. (a) Plots of the D_{pB}/D_{pG} ratio against % (v/v) of crowding agents (black circle: EG, red circle: PEG 400, yellow circle: PEG 8000, green circle: Ficoll PM 70, and blue circle: Dextran 40). (b) Plots of the ΔR_h values against the mole fraction (X_i) of molecular crowding agents (black circle: EG, red circle: PEG 400, yellow circle: PEG 8000, green circle: Ficoll PM 70, and blue circle: Dextran 40).

ing; Ramachandran et al. suggested that the I_2' state (also referred to as the pB_2 state) has a comparatively well-ordered and rearranged conformation, which has an increased R_g value and an increased maximum dimension.[19] They also demonstrated that in the I_2' state a portion of the N-terminal domain contacts the exposed cleft of the chromophore-binding domain, whereas the remaining terminal residues extend away from the core.[19] In addition, in another study of PYP using time-resolved X-ray solution scattering, Kim et al. suggested that the N-terminus of PYP protrudes during the photocycle of PYP and that the increase in the volume of the protein is maximized in the final intermediate, pB_2.[20] These results constitute evidence

DOI: 10.1021/acs.jpcb.6b13076
J. Phys. Chem. B 2017, 121, 769−779

for the occurrence of a large molecular volume change accompanying the formation of the pB_2 state.

The D_{pG} and D_{pB} values in the presence of molecular crowding agents were also determined by quantitatively analyzing the TG signals using eq 1. The values determined for D_{pG} and D_{pB} in the presence of molecular crowding agents are summarized in Tables 1 and 2. Generally, an increase in the mass concentration of molecular crowding agents induces an increase in the solution viscosity.[11,37−40] However, with the increasing solvent viscosity upon addition of molecular crowding agents, the decrease in both D_{pG} and D_{pB} values clearly deviates from linearity (not shown). This deviation indicates that the photoinduced conformational change of PYP in the presence of molecular crowding agents is affected by the additional effect such as the excluded volume effect or dehydration as well as the solution viscosity.

Interestingly, upon addition of molecular crowding agents, the D_{pB} value becomes close to the D_{pG} value, as depicted in Tables 1 and 2 and Figure 3a. That is, the D_{pB}/D_{pG} ratio converges to 1.0 as the concentration of molecular crowding agents increases (see Figure 3a). The diffusion coefficient is directly related to the hydrodynamic radius (R_h) of a chemical species. Thus, the similarity between the D_{pG} and D_{pB} values implies that the pG and pB species have a similar molecular volume (and/or shape) in molecular crowding environments. In other words, this means that the photocycling of PYP in molecularly crowded environments does not involve a large conformational change in the protein, particularly in terms of R_h. Empirically, the small molecular volume change occurring during the photocycle of PYP upon addition of molecular crowding agents is reflected in the intensities of the TG signals. The peak in the latest time region in the TG signals (Figures 2 and S8) is due to the diffusion processes of both pG and pB. The peak intensities gradually decrease upon addition of molecular crowding agents. Typically, as shown in eq 1, the species grating intensity in TG experiments is related to the diffusion coefficients of the reactant and the product, as well as the difference between δn values (δn_R and δn_P) due to changes in the concentration of the reactant and the product. The sign of δn_P is positive, whereas the sign of δn_R is negative because the phase of the spatial concentration modulation of the product is shifted 180° from that of the reactant. During the photocycle of PYP, pB is the detected photoproduct and pG is the reactant. As mentioned above, upon addition of molecular crowding agents, the D_{pB} value becomes close to the D_{pG} value ($D_{pG} \approx D_{pB}$). Thus, two terms of $\delta n_{pG} \exp(-D_{pG}q^2t)$ and $\delta n_{pB} \exp(-D_{pB}q^2t)$ are canceled. Consequently, the intensity of the peak becomes weaker in molecularly crowded environments because of the opposite signs of δn_{pG} and δn_{pB}. As mentioned above, meanwhile, PYP in the presence of BSA showed a new weak TG signal in the longer time region. This weak TG signal that depends on the q-value (Figure S10) was fitted using the following function

$$I_{TG} = \left[\delta n_1 \exp\left(-\frac{t}{\tau_1}\right) + \delta n_{th} \exp(-D_{th}q^2t) + \delta n_2 \exp\left(-\frac{t}{\tau_2}\right) + \delta n_3 \exp\left(-\frac{t}{\tau_3}\right) - \delta n_{pG} \exp(-D_{pG}q^2t) + \delta n_{pB} \exp(-D_{pB}q^2t) + \delta n_X \exp(-D_Xq^2t)\right]^2 \quad (2)$$

where δn_X is the refractive index change due to the change in the concentration of a new species X during the reaction and D_X is the diffusion coefficient of the species X. From the quantitative analysis of TG signals measured in the presence of BSA, the D_X value in the presence of 200 g/L BSA is determined to be 2.7×10^{-11} m^2 s^{-1}. This D_X value is greatly smaller than that of pG and pB. Considering the small D_X value, we tentatively assign the chemical species of this small D_X to the PYP−BSA complex formed by the interaction between PYP and BSA. This result is in contrast to that of previous studies, showing that BSA is an inert molecule for various biomolecules.[2,29−32] However, it is not clear how PYP interacts with BSA during its photocycle.

To confirm the small photoinduced molecular volume change of PYP within cell-mimetic environments, the change in the R_h value upon pG → pB transition was calculated from D_{pG} and D_{pB} observed in the cell-mimetic environment. Previous studies on the photocycle of PYP revealed that in the absence of molecular crowding agents the formation of the pB state induces the largest conformational change, resulting from the partial unfolding of α-helices in the N-terminal region.[26,28] Khan et al. revealed that the unfolding of an α-helix in the N-terminal region upon formation of the pB state can be determined by measuring differences in the frictional coefficient ($\Delta f = k_BT(1/D_{pB} - 1/D_{pG})$).[26] Considering the Stokes−Einstein relationship, the Δf value can be expressed as follows

$$\Delta f = 6\pi\eta(R_{h\text{-}pB} - R_{h\text{-}pG}) \quad (3)$$

where η is the viscosity of solutions, and $R_{h\text{-}pB}$ and $R_{h\text{-}pG}$ are the hydrodynamic radii of pB and pG, respectively. The change in the hydrodynamic radius upon pG → pB transition within the cell-mimetic environment was calculated using eq 3, and the values are listed in Tables 1 and 2. The ΔR_h ($R_{h\text{-}pB} - R_{h\text{-}pG}$) value is calculated to be 1.68 ± 0.08 Å in the absence of molecular crowding agents. As shown in Tables 1 and 2 and Figure 3b, ΔR_h decreases as the concentration of molecular crowding agents increases, supporting the inference that the photocycle of PYP in molecularly crowded environments does not induce a large molecular volume change of the protein. Definitely, the ΔR_h values decrease more steeply with the addition of large crowding agents such as PEG 8000, Ficoll PM 70, and Dextran 40 than with small crowing agents such as EG and PEG 400 (Figure 3b). It is known that macromolecules with a large molecular size and weight produce a larger excluded volume[41] and that the excluded volume effect becomes more significant when the introduced biomolecule has a similar size to that of the molecular crowding agent.[1,4] The sizes of PEG 8000, Ficoll PM 70, and Dextran 40 are larger than those of PYP (R_g = 15.2 Å); R_g of PYP: 15.2 Å, R_g of PEG 8000: 16.0 Å,[42] R_g of Ficoll PM 70: 41.5 Å,[43] and R_g of Dextran 40: 62 Å.[44] Considering the molecular sizes of PYP and these

DOI: 10.1021/acs.jpcb.6b13076
J. Phys. Chem. B 2017, 121, 769−779

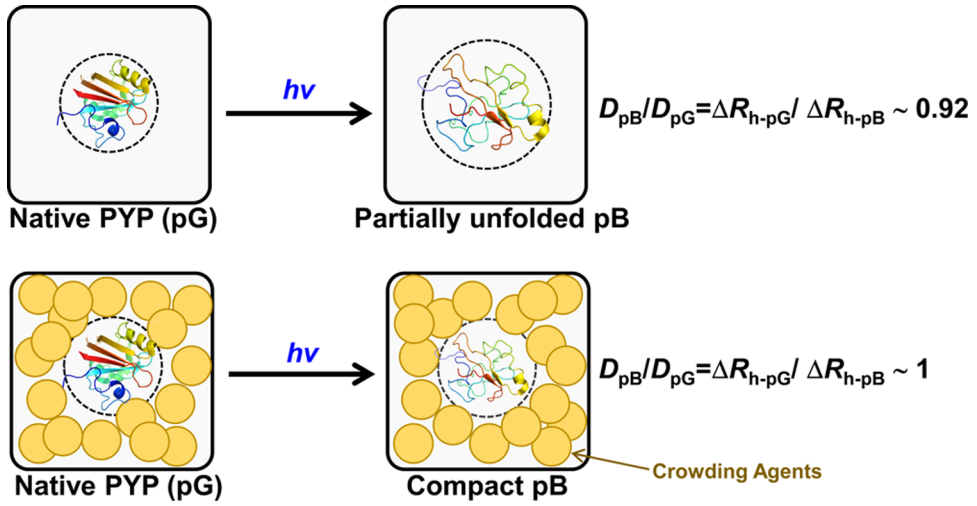

Figure 4. Schematic illustration for molecular crowding effect. Photoinduced conformational change of PYP in the absence (top) and presence (bottom) of molecular crowding agents. Structures of pG (PDB ID: 3PHY) and pB (PDB ID: 2KX6).

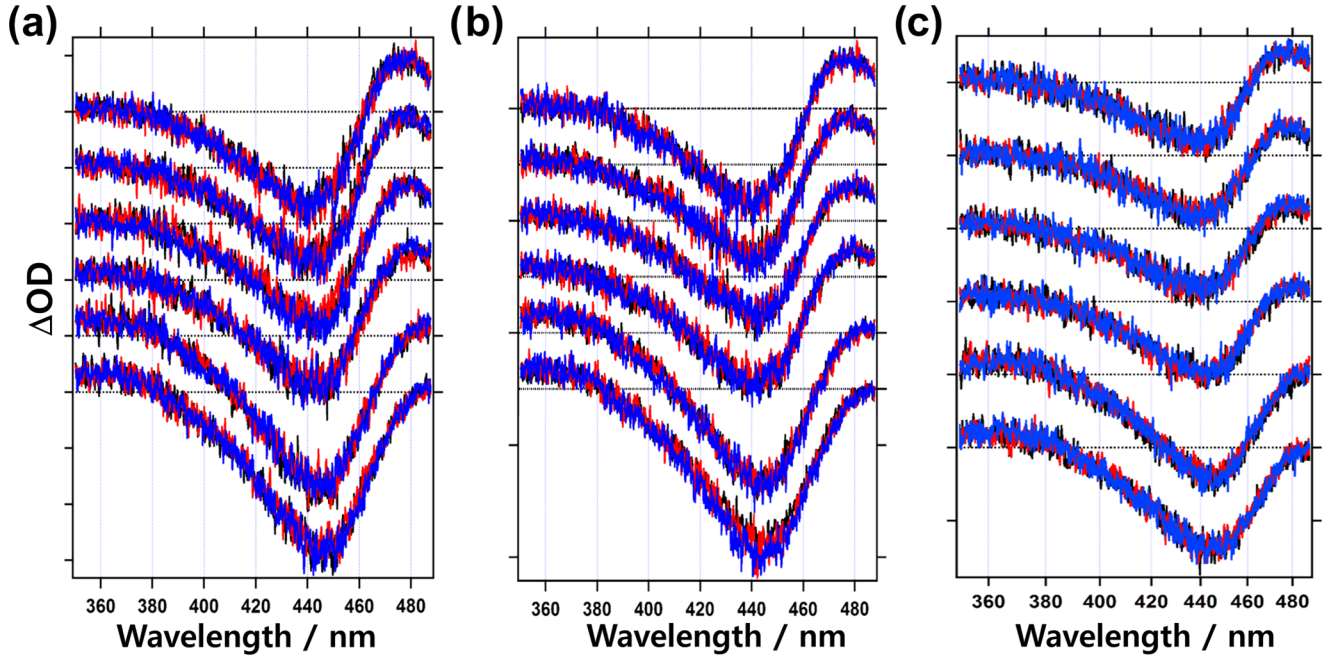

Figure 5. TA spectra of PYP in the presence of EG (a), PEG 400 (b), and (c) Ficoll PM 70. (a) TA spectra of PYP in 0 (black), 10 (red), and 20% (v/v) (blue) EG solutions. (b) TA spectra of PYP in 0% (v/v) (black), 10% (v/v) (red), and 20% (v/v) (blue) PEG 400 solutions. (c) TA spectra of PYP in 0% (v/v) (black), 4% (v/v) (red), and 8% (v/v) (blue) Ficoll PM 70 solutions. All TA spectra of PYP in the presence of molecular crowding agents at selected time points are shown (from top to bottom: 100 ns, 1 μs, 10 μs, 100 μs, 1 ms, and 10 ms).

crowding agents, PEG 8000, Ficoll PM 70, and Dextran 40 should produce a larger excluded volume effect than EG or PEG 400. Consequently, the volume available to the pG and pB species in the presence of PEG 8000, Ficoll PM 70, and Dextran 40 is much less than what is available in the presence of the small crowding agents, resulting in an inhibition of large molecular volume changes. These results suggest that the intermediate formed during the photocycle of PYP favors a compact conformation under physiological conditions as schematically shown in Figure 4 and that the excluded volume effect is responsible for such a suppressed molecular volume change in crowded environments. This leads to the hypothesis that the signaling activity of PYP cannot be mediated solely by the large conformational changes upon formation of pB.

Kinetics on the Photocycle of PYP. To elucidate the photocycle of PYP in molecular crowding environments, TA signals of PYP in the presence of various crowding agents were measured. Figure 5 shows the representative TA signals of PYP in 50 mM Tris−HCl buffer (pH 7) as a function of the concentration of EG, PEG 400, and Ficoll PM 70. PYP in the absence of crowding agents shows positive absorption signals at around 370 and 480 nm and a broad bleaching signal at 446 nm due to the absorption band of pG. TA absorption signals at around 370 and 480 nm are attributed mainly to the formation of pB and pR, respectively. As shown in Figures 5 and S11, TA spectrum of PYP at each time delay is hardly affected by the addition of molecular crowding agents. These results indicate that the photocyclic reaction of PYP is not influenced by the

DOI: 10.1021/acs.jpcb.6b13076
J. Phys. Chem. B 2017, 121, 769−779

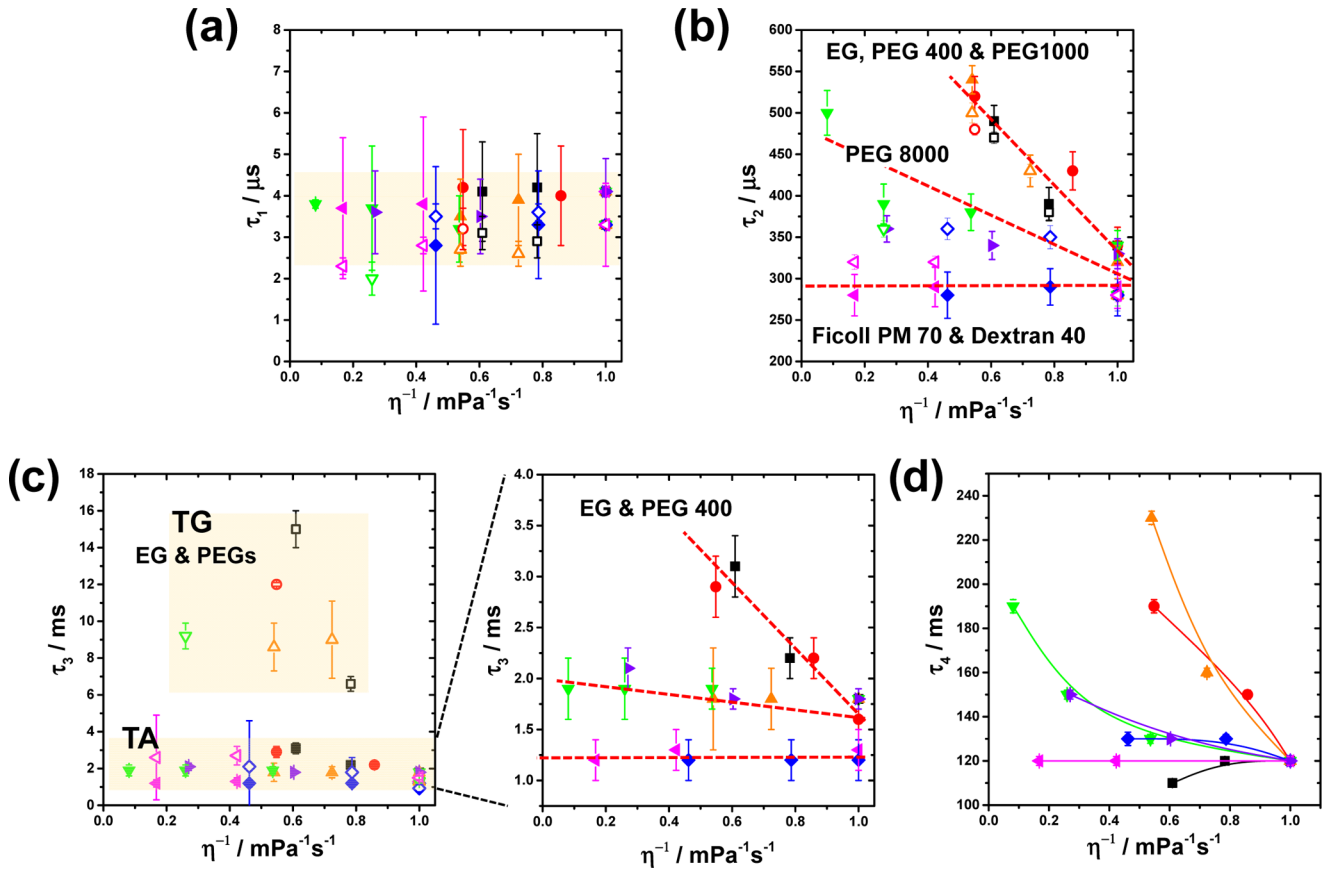

Figure 6. Time constants for the photocycle of PYP obtained from TA and TG experiments. (a–d) Plots for τ_1, τ_2, τ_3, and τ_4 against the reciprocal of the solution viscosity, respectively. The solid and open symbols denote the time constants determined by TA and TG experiments, respectively. The black, red, orange, green, blue, pink, and purple symbols indicate the time constants for the photocycle of PYP obtained in the presence of EG, PEG 400, PEG 1000, PEG 8000, Ficoll PM 70, Dextran 40, and BSA, respectively.

addition of molecular crowding agents, as suggested by TG experiments. The temporal profiles of the TA signal of PYP in the absence and presence of molecular crowding agents were measured at 362, 446, and 477 nm. All decay profiles were well-reproduced by a tetra-exponential function as shown in Figures S12 and S13. The time constants determined from the global fitting are summarized in Table S2. Although, as shown in Table S2 and Figure 6, the four time constants show slightly different dependence on each crowding agent, the trend in the kinetics of the photocycle of PYP determined by TA experiments is very similar to that observed by TG experiments. The τ_1 values are not affected by the addition of molecular agents. The τ_2, τ_3, and τ_4 values are decelerated mainly by the addition of EG and PEGs, whereas large crowding agents such as Ficoll PM 70, Dextran 40, and BSA do not affect the kinetics on the photocycle of PYP. Hellingwerf and co-workers demonstrated that the faster dark recovery of pG in the crystal phase comes from the compact structure of the intermediate compared to that in the solution phase.[15] In this regard, our results show that even though pB has a compact structure in molecularly crowding environments generated by Ficoll PM 70, Dextran 40, and BSA, the kinetics on the photocycle of PYP is barely influenced unlike in the case of crystalline environment.

The τ_1 measured by the TA and TG techniques shows constant values regardless of the solution viscosity as depicted in Figure 6a, indicating that the dynamics corresponding to τ_1 is independent of the solution viscosity. This result means that the conformational change occurring within a few microsecond time scale is so small that the influence of the solution viscosity is negligible. The τ_1 in the sequential kinetic model is assigned to the $pR_1 \rightarrow pR_2$ transition,[26−28] whereas in the parallel model, the τ_1 is assigned to the $pR_1 \rightarrow pB_1$ transition.[20,21,45] The τ_1 with a time constant of ∼1 μs does not accompany a noticeable spectral change. In the sequential model, this lack of spectral change is rationalized by suggesting that the $pR_1 \rightarrow pR_2$ transition accompanies the conformational change far from the chromophore.[28,46] On the other hand, in the parallel model, the negligible spectral change in the visible TA and infrared absorption measurements are explained by noting that the orientation of the chromophore and the surrounding hydrogen-bonding network in the pB_1 state are very similar to those in the pR_1 state.[20] Kim et al. revealed that although the protrusion of the N-terminus in the pR_2 state is much less than that of the other intermediates (pR_1, pB_1, and pB_2), both transitions, $pR_1 \rightarrow pR_2$ in the sequential model and $pR_1 \rightarrow pB_1$ in the parallel model, induce a small decrease in the radius of gyration (R_g) value; from 15.13 to 15.07 Å in the sequential model and from 15.4 to 15.26 Å in the parallel model.[20] These previous results support our suggestion that the conformational change occurring within a few microsecond time scale is very small or negligible.

Both τ_2 and τ_3 values are assigned to the $pR_2 \rightarrow pB_1$ and the $pB_1 \rightarrow pB_2$ transition, respectively. It is known that the $pB_1 \rightarrow pB_2$ transition induces the conformational change in the β-sheet domain, whereas the $pR_2 \rightarrow pB_1$ transition results in the conformational change in the N-terminal region accompanied

DOI: 10.1021/acs.jpcb.6b13076
J. Phys. Chem. B 2017, 121, 769−779

with the protonation of *p*CA.[28] Especially, the $pB_1 \rightarrow pB_2$ transition induces the largest conformational change due to the partial unfolding of the N-terminus.[20,26,28] Therefore, both transitions, which induce the tertiary structural change of a protein, should be influenced by changes in the solution viscosity upon addition of molecular crowding agents. Generally, the solution viscosity is greatly affected by the crowding agents with a high MW rather than by those with a low MW.[11,37−40] However, as shown in Figure 6b,c, both τ_2 and τ_3 values are greatly affected by the addition of crowding agents with a low MW (EG, PEG 400, and PEG 1000) but not by crowding agents with high MW and size, such as PEG 8000, Ficoll PM 70, Dextran 40, and BSA. Thus, these results indicate that upon addition of molecular crowding agents, the deceleration for both $pR_2 \rightarrow pB_1$ and $pB_1 \rightarrow pB_2$ transitions is probably due to the dehydration owing to the release of protein-binding water molecules but not due to the solution viscosity. As explained above, molecular crowding agents with a low MW; such as EG, PEG 400, and PEG 1000; can also act as strong dehydration agents, which can induce the release of protein-binding water molecules.[4,41] This observation of deceleration due to dehydration is consistent with that the pB_2 formation in the crystalline phase (23 ms) is significantly slow compared to that in the solution phase as observed using time-resolved Laue X-ray crystallography.[45] Kaledhonkar reported that the hydration level of a protein in the crystalline phase is lower than that in the solution phase, consequently leading to the deceleration of the conformational dynamics of a protein.[47] These previous studies support our suggestion that the deceleration for both $pR_2 \rightarrow pB_1$ and $pB_1 \rightarrow pB_2$ transitions comes from the dehydration owing to the release of protein-binding water molecules.

Meanwhile, it is interesting to compare the τ_3 values determined by both TG and TA experiments. In the presence of molecular crowding agents with a small molecular size, the time constants for the pB_2 formation determined by TG experiments are significantly slower than those determined by TA experiments (see Tables S1 and S2 and Figure 6). This discrepancy for the $pB_1 \rightarrow pB_2$ transition can be interpreted by the features of both techniques. The TG technique has a high sensitivity for the tertiary and quaternary structural changes of a protein, whereas the TA technique is sensitive to the structural change of a chromophore and nearby residues. From this point of view, the discrepancy in time constants for the $pB_1 \rightarrow pB_2$ transition observed by both TG and TA techniques is probably due to the difference in time scales corresponding to the global conformational change of a protein and the structural change occurring nearby a chromophore. Therefore, we suggest that in the presence of crowding agents such as EG, PEG 400, and PEG 1000, the global conformational change accompanied by the $pB_1 \rightarrow pB_2$ transition in molecularly crowded environments is much slower than the local structural change occurring around the chromophore. A similar result was reported by Choi and Terazima.[48] They demonstrated that the deformation of the tertiary structure of myoglobin occurs slowly relative to the unfolding of the secondary structure, α-helices, indicating that the global structure of Mb is still changing after the secondary structure deformation process.[48]

Finally, as shown in Figure 6d and Tables S1 and S2, the τ_4, the dark recovery time of pB_2, is decelerated by the addition of PEG 400, PEG 1000, and PEG 8000, whereas the addition of EG, Ficoll PM 70, Dextran 40, and BSA does not affect the dark recovery process of pB_2. This result is consistent with that reported by Hellingwerf and co-workers.[15] Harigai et al. suggested that the electrostatic interactions between the N-terminus and the β-sheet play an important role in the dark recovery process of pB_2.[36] Indeed, they demonstrated that the slower dark recovery time observed for N-terminal truncated PYPs is due to the lack of the electrostatic interactions between the N-terminus and the β-sheet. In this study, using NMR experiments for uniformly ^{15}N-labeled PYP, we found that PEG 400 nonspecifically interacts with the residues in loop regions and in N-terminal helical regions and near the water cavity in internally structured regions (Figures S2−S6). This binding of PEGs in N-terminal helical regions should decrease the electrostatic interactions between the N-terminus and the β-sheet, resulting in the deceleration of the dark recovery time of pB_2.

CONCLUSIONS

PYP is a model system for studying light sensing and signal transduction. Numerous studies have shown that the photocycle of PYP accompanies a large molecular volume change (or conformational change) in vitro upon absorption of blue light. However, the photocycle of PYP in physiological conditions containing a number of other highly concentrated species, such as biomolecules and ions, is still unclear. Here, the photocycle of PYP in a cell-mimetic environment was investigated using various spectroscopic techniques, such as UV−vis, CD, NMR, TA, and TG techniques. Surprisingly, upon addition of molecular crowding agents, the value of D_{pB} approaches that of D_{pG}, indicating that, under molecularly crowded conditions, pB has a similar degree of compactness as that of pG (see Figure 4). Indeed, the ΔR_h value induced by the photocycle of PYP is significantly decreased with increasing concentrations of molecular crowding agents. The decrease in ΔR_h value is more clearly observed when the large molecular crowding agents, such as PEG 8000, Ficoll PM 70, and Dextran 40, are used. On the other hand, the kinetics on the photocycle of PYP is decelerated mainly by the addition of EG and PEGs, whereas large crowding agents, such as Ficoll PM 70, Dextran 40, and BSA, do not affect the kinetics on the photocycle of PYP. The results presented in this study clearly demonstrate that the molecular volume change accompanied by the photocycle of PYP in molecularly crowded environments is significantly influenced by the excluded volume effect, whereas the kinetics of the photocycle of PYP is greatly affected by the dehydration rather than the excluded volume effect.

The study of molecular crowding effect on the photocycle of PYP suggests that the conformational change of PYP upon irradiation of blue light in vivo is smaller than that observed in vitro, which leads us to hypothesize that the putative signaling transducer of PYP cannot detect the signal by relying solely on the changes in the conformation of pB.

MATERIALS AND METHODS

PYP Sample Preparation. The gene encoding PYP in *H. halophila* was amplified by PCR using the pQE80L-EK-PYP plasmid [1] as the template DNA. The amplified DNA was cloned into a pET-His_6-TEV-LIC cloning vector (2B-T), which was a gift from Prof. Scott Gradia (Addgene plasmid # 29666). The protein was expressed in *Escherichia coli* BL21 (DE3) at 37 °C. The chromophore (*p*CA) was incorporated prior to cell disruption. The supernatant was subject to Ni Sepharose 6 Fast Flow (GE Healthcare). The protein was eluted with 20 mM

DOI: 10.1021/acs.jpcb.6b13076
J. Phys. Chem. B 2017, 121, 769−779

Tris−HCl, pH 8.0, 50 mM NaCl, 250 mM imidazole. The N-terminal hexahistidine tag was cleaved by TEV digestion during dialysis against 20 mM Tris−HCl, pH 8.0, 50 mM NaCl, 1 mM DTT. The protein was purified further by a Q-Sepharose column (GE Healthcare), using a linear gradient of 50 mM to 1 M NaCl. The protein fractions that had the purity index, the ratio between the absorbances at 280 and 446 nm, approximately equal to 0.43 were collected, dialyzed against 50 mM Tris−HCl, pH 7.0, 25 mM NaCl, and concentrated to 2 mM for further studies.

Preparation of PYP Samples with Various Concentrations of Crowding Reagents. EG and PEG 400 (MW: ∼400) were purchased from Tokyo Chemical Industry Co., and PEG 1000 (MW: ∼1000) and PEG 8000 (MW: ∼8000) were purchased from Hampton Research. Ficoll PM 70 (MW: ∼70 000) and Dextran 40 (MW: ∼40 000) were purchased from Sigma-Aldrich Co. PYP samples containing 0, 2, 4, 6, 8, 10, 15, 20, 30, and 40% v/v of each crowding reagent were prepared by direct dilution of the 2 mM PYP protein stock with solutions of the crowding reagents, adjusting the concentration of Tris−HCl, pH 7.0 and NaCl using a 1 M Tris−HCl, pH 7.0 and a 5 M NaCl stock solution.

UV−Vis and CD Spectroscopy. Samples of PYP (60 μM) were prepared with various concentrations of crowding reagents as described above. UV−vis spectra were measured using a UV−vis spectrometer (UV-2550; Shimadzu, Japan) with a 1 cm quartz cuvette at room temperature. CD spectra were measured using a CD spectrometer (Jasco-815; JASCO, Japan) with a 0.1 mm quartz cuvette at room temperature.

TG Experiments. The setup for TG experiments was similar to that reported in our previous work.[33−35] Briefly, a 460 nm pulsed laser beam from an optical parametric oscillator (LT-2144-PC; LOTIS TII, Belarus) pumped by an Nd:YAG laser (NL301G; EKSPLA, Lithuania) was split into two equivalent beams. The two excitation beams and the 830 nm continuous-wave laser beam intersected each other on the sample. The diffracted signal was isolated from other beams by using a longpass filter (>780 nm) and detected by a combination of a photomultiplier tube (PMT) module (Hamamatsu, Japan) and a digital oscilloscope (Tektronix, U.S.A.). The repetition rate of the excitation beam was 0.5 Hz. The total energy of the excitation beams was adjusted to be under ∼15 μJ to avoid any photodamage or signal saturation. The excitation beam size was focused to a diameter of ∼1 mm at the sample position. The concentration of PYP in the test samples was adjusted to be ∼340 μM. The sample solution was contained in a quartz cell (2 mm path length; Starna Scientific, U.K.). TG signals were measured from PYP samples, with varying concentrations of the crowding agents, at a single grating wavenumber, q. The q-values were determined from the TG signal of the reference sample, bromocresol purple (BCP). As BCP releases the entirety of its photoexcitation energy as heat, only the thermal diffusion process is observed in the TG signal of BCP. From the rate constants of the thermal diffusion of the BCP sample, the q-value corresponding to each alignment was determined.

TA Experiment. Experimental setup for TA measurement was similar to that reported in our previous work.[33−35] Briefly, the probe white light (continuous wave) was got through the sample position in an angle as acute as possible against the 460 nm pump laser beam to maximize the overlap between pump and probe beams. The TA signal was detected by the combination of a spectrometer (ACTON 2300i; Princeton Instruments, U.S.A.) and an ICCD (iStar; Andor Technology, U.K.) or a PMT. The concentrations of PYPs were adjusted to be about 70 μM. The sample solution was flowed using a syringe pump (Legato 111; KD Scientific, U.S.A.) and a flow cell with 2 mm path length. The repetition rate of the pump beam was 0.5 or 1 Hz.

Preparation of ^{15}N-Labeled Samples and NMR Experiments. Uniformly ^{15}N-labeled PYP was expressed in *E. coli* BL21(DE3) using M9 minimal media, with $^{15}NH_4Cl$ as the sole nitrogen source. The recombinant protein was purified as described previously. ^{15}N-labeled PYP samples containing differing concentrations of PEG 400 (0, 2, 6, 10, 20, 30, and 40% v/v) were prepared as described previously. All samples contained the same concentration of Tris−HCl, pH 7.0, NaCl, and 10% D_2O, except those containing PEG 400. NMR experiments were performed on a Bruker Avance 700 MHz spectrometer (KBSI, Korea).

NMR Data Processing and Analysis. NMR spectra were processed with *NMRPipe*[49] and analyzed and visualized by *Sparky*.[50] Chemical shifts of the amide protons in PYP in the absence of molecular crowding reagents were manually assigned on the basis of the BMRB entry: 18122.[51] Chemical shift perturbations (CSPs) were calculated as follows

$$\mathrm{CSP}(\Delta\delta) = \sqrt{\frac{1}{2}\cdot[\delta_H{}^2 + \alpha\cdot\delta_N{}^2]}$$

In the equation above, $\Delta\delta$ is the chemical shift perturbation (ppm), δ_H is the chemical shift difference along the proton axis, δ_N is the chemical shift difference along the nitrogen axis, and α is a weighting factor with a value of 0.15. The calculated CSP was plotted versus residue numbers (Figure 2b), mapped onto a crystal structure (PDB: 2PHY)[52] and a solution structure of PYP (PDB: 3PHY),[53] and visualized using *PYMOL*.

SAXS Experiments. PYP samples (0.5 mM) were prepared with various concentrations of PEG 400 (0, 10, 20, 30, and 40% v/v). All samples were centrifuged at 14 000 rpm for 10 min before collecting data. The collection of SAXS data was conducted at the 4C SAXS II beamline (Pohang Accelerator Laboratory; PAL, Korea). All SAXS measurements were done with a 10 time exposure, at room temperature in a flow cell system (1 mm capillary, flow rate: 15 μL/min). The exposure time was 60 s for each individual measurement. Several X-ray scattering datasets were collected for PYP in crowded environments and for the corresponding buffers without PYP. To determine the R_g value of PYP, the scattering signals from the buffer containing various concentrations of PEG 400 were subtracted from those of the PYP in the solutions containing the corresponding concentrations of PEG 400. All data were processed, merged, and analyzed using *ATSAS* software.[54] R_g values for the sample were derived from the SAXS data ($q_{max} \times R_g \leq 1.15$).

■ ASSOCIATED CONTENT

Supporting Information

The Supporting Information is available free of charge on the ACS Publications website at DOI: 10.1021/acs.jpcb.6b13076.

UV−vis and CD spectroscopic measurements; NMR spectroscopic analysis; SAXS measurements; TG signals and TA spectra for PYP in the presence of various crowding agents (PDF)

DOI: 10.1021/acs.jpcb.6b13076
J. Phys. Chem. B 2017, 121, 769−779

AUTHOR INFORMATION

Corresponding Authors

*E-mail: jkchoi@ibs.re.kr (J.C.).
*E-mail: hyotcherl.ihee@kaist.ac.kr (H.I.).

ORCID

Hyotcherl Ihee: 0000-0003-0397-5965

Author Contributions

§C.Y. and S.O.K. contributed equally.

Notes

The authors declare no competing financial interest.

ACKNOWLEDGMENTS

We thank the beamline staffs at the Pohang Accelerator Laboratory (PAL, Korea) for assistance with SAXS data collection. We also thank Dr. K. Yeo for helping the measurement of NMR spectra. This work was supported by IBS-R004-G2.

REFERENCES

(1) Ellis, R. J. Macromolecular Crowding: Obvious but Underappreciated. *Trends Biochem. Sci.* **2001**, *26*, 597−604.
(2) Zhou, H. X.; Rivas, G.; Minton, A. P. Macromolecular Crowding and Confinement: Biochemical, Biophysical, and Potential Physiological Consequences. *Annu. Rev. Biophys.* **2008**, *37*, 375−397.
(3) Zimmerman, S. B.; Trach, S. O. Estimation of Macromolecule Concentrations and Excluded Volume Effects for the Cytoplasm of *Escherichia Coli*. *J. Mol. Biol.* **1991**, *222*, 599−620.
(4) Miyoshi, D.; Sugimoto, N. Molecular Crowding Effects on Structure and Stability of DNA. *Biochimie* **2008**, *90*, 1040−1051.
(5) Krotova, M. K.; Vasilevskaya, V. V.; Makita, N.; Yoshikawa, K.; Khokhlov, A. R. DNA Compaction in a Crowded Environment with Negatively Charged Proteins. *Phys. Rev. Lett.* **2010**, *105*, No. 128302.
(6) Benton, L. A.; Smith, A. E.; Young, G. B.; Pielak, G. J. Unexpected Effects of Macromolecular Crowding on Protein Stability. *Biochemistry* **2012**, *51*, 9773−9775.
(7) Cheung, M. S.; Klimov, D.; Thirumalai, D. Molecular Crowding Enhances Native State Stability and Refolding Rates of Globular Proteins. *Proc. Natl. Acad. Sci. U.S.A.* **2005**, *102*, 4753−4758.
(8) Tokuriki, N.; Kinjo, M.; Negi, S.; Hoshino, M.; Goto, Y.; Urabe, I.; Yomo, T. Protein Folding by the Effects of Macromolecular Crowding. *Protein Sci.* **2004**, *13*, 125−133.
(9) Gomez, D.; Klumpp, S. Biochemical Reactions in Crowded Environments: Revisiting the Effects of Volume Exclusion with Simulations. *Front. Phys.* **2015**, *3*, 45.
(10) Tabaka, M.; Kalwarczyk, T.; Szymanski, J.; Hou, S.; Holyst, R. The Effect of Macromolecular Crowding on Mobility of Biomolecules, Association Kinetics and Gene Expression in Living Cells. *Front. Phys.* **2014**, *2*, 119.
(11) Kozer, N.; Kuttner, Y. Y.; Haran, G.; Schreiber, G. Protein-Protein Association in Polymer Solutions: From Dilute to Semidilute to Concentrated. *Biophys. J.* **2007**, *92*, 2139−2149.
(12) Meyer, T. E.; Yakali, E.; Cusanovich, M. A.; Tollin, G. Properties of a Water-Soluble, Yellow Protein Isolated from a Halophilic Phototrophic Bacterium that has Photochemical Activity Analogous to Sensory Rhodopsin. *Biochemistry* **1987**, *26*, 418−423.
(13) Hoff, W. D.; van Stokkum, I. H.; van Ramesdonk, H. J.; van Brederode, M. E.; Brouwer, A. M.; Fitch, J. C.; Meyer, T. E.; van Grondelle, R.; Hellingwerf, K. J. Measurement and Global Analysis of the Absorbance Changes in the Photocycle of the Photoactive Yellow Protein from Ectothiorhodospira Halophila. *Biophys. J.* **1994**, *67*, 1691−1705.
(14) Hendriks, J.; Hoff, W. D.; Crielaard, W.; Hellingwerf, K. J. Protonation/Deprotonation Reactions Triggered by Photoactivation of Photoactive Yellow Protein from Ectothiorhodospira Halophila. *J. Biol. Chem.* **1999**, *274*, 17655−17660.
(15) Yeremenko, S.; van Stokkum, I. H.; Moffat, K.; Hellingwerf, K. J. Influence of the Crystalline State on Photoinduced Dynamics of Photoactive Yellow Protein Studied by Ultraviolet-Visible Transient Absorption Spectroscopy. *Biophys. J.* **2006**, *90*, 4224−4235.
(16) Imamoto, Y.; Kataoka, M. Structure and Photoreaction of Photoactive Yellow Protein, a Structural Prototype of the PAS Domain Superfamily. *Photochem. Photobiol.* **2007**, *83*, 40−49.
(17) van der Horst, M. A.; Stalcup, T. P.; Kaledhonkar, S.; Kumauchi, M.; Hara, M.; Xie, A.; Hellingwerf, K. J.; Hoff, W. D. Locked Chromophore Analogs Reveal that Photoactive Yellow Protein Regulates Biofilm Formation in the Deep Sea Bacterium Idiomarina Loihiensis. *J. Am. Chem. Soc.* **2009**, *131*, 17443−17451.
(18) Yamaguchi, S.; Kamikubo, H.; Kurihara, K.; Kuroki, R.; Niimura, N.; Shimizu, N.; Yamazaki, Y.; Kataoka, M. Low-Barrier Hydrogen Bond in Photoactive Yellow Protein. *Proc. Natl. Acad. Sci. U.S.A* **2009**, *106*, 440−444.
(19) Ramachandran, P. L.; Lovett, J. E.; Carl, P. J.; Cammarata, M.; Lee, J. H.; Jung, Y. O.; Ihee, H.; Timmel, C. R.; van Thor, J. J. The Short-Lived Signaling State of the Photoactive Yellow Protein Photoreceptor Revealed by Combined Structural Probes. *J. Am. Chem. Soc.* **2011**, *133*, 9395−9404.
(20) Kim, T. W.; Lee, J. H.; Choi, J.; Kim, K. H.; van Wilderen, L. J.; Guerin, L.; Kim, Y.; Jung, Y. O.; Yang, C.; Kim, J.; et al. Protein Structural Dynamics of Photoactive Yellow Protein in Solution Revealed by Pump-Probe X-ray Solution Scattering. *J. Am. Chem. Soc.* **2012**, *134*, 3145−3153.
(21) Jung, Y. O.; Lee, J. H.; Kim, J.; Schmidt, M.; Moffat, K.; Srajer, V.; Ihee, H. Volume-Conserving Trans-Cis Isomerization Pathways in Photoactive Yellow Protein Visualized by Picosecond X-ray Crystallography. *Nat. Chem.* **2013**, *5*, 212−220.
(22) Jung, Y. O.; Lee, J. H.; Kim, J.; Schmidt, M.; Moffat, K.; Srajer, V.; Ihee, H. Reply to 'Contradictions in X-ray Structures of Intermediates in the Photocycle of Photoactive Yellow Protein'. *Nat. Chem.* **2014**, *6*, 259−260.
(23) Kim, J. G.; Kim, T. W.; Kim, J.; Ihee, H. Protein Structural Dynamics Revealed by Time-Resolved X-ray Solution Scattering. *Acc. Chem. Res.* **2015**, *48*, 2200−2208.
(24) Tamura, K.; Hayashi, S. Role of Bulk Water Environment in Regulation of Functional Hydrogen-Bond Network in Photoactive Yellow Protein. *J. Phys. Chem. B* **2015**, *119*, 15537−15549.
(25) Imamoto, Y.; Kamikubo, H.; Harigai, M.; Shimizu, N.; Kataoka, M. Light-Induced Global Conformational Change of Photoactive Yellow Protein in Solution. *Biochemistry* **2002**, *41*, 13595−13601.
(26) Khan, J. S.; Imamoto, Y.; Harigai, M.; Kataoka, M.; Terazima, M. Conformational Changes of PYP Monitored by Diffusion Coefficient: Effect of N-terminal Alpha-Helices. *Biophys. J.* **2006**, *90*, 3686−3693.
(27) Schotte, F.; Cho, H. S.; Kaila, V. R.; Kamikubo, H.; Dashdorj, N.; Henry, E. R.; Graber, T. J.; Henning, R.; Wulff, M.; Hummer, G.; et al. Watching a Signaling Protein Function in Real Time via 100-ps Time-Resolved Laue Crystallography. *Proc. Natl. Acad. Sci. U.S.A.* **2012**, *109*, 19256−19261.
(28) Hoshihara, Y.; Imamoto, Y.; Kataoka, M.; Tokunaga, F.; Terazima, M. Conformational Changes in the N-terminal Region of Photoactive Yellow Protein: A Time-Resolved Diffusion study. *Biophys. J.* **2008**, *94*, 2187−2193.
(29) Laurent, T. C. The Interaction between Polysaccharides and Other Macromolecules. 5. The Solubility of Proteins in the Presence of Dextran. *Biochem. J.* **1963**, *89*, 253−257.
(30) Rivas, G.; Fernandez, J. A.; Minton, A. P. Direct Observation of the Enhancement of Noncooperative Protein Self-Assembly by Macromolecular Crowding: Indefinite Linear Self-Association of Bacterial Cell Division Protein FtsZ. *Proc. Natl. Acad. Sci. U.S.A.* **2001**, *98*, 3150−3155.
(31) Sasahara, K.; McPhie, P.; Minton, A. P. Effect of Dextran on Protein Stability and Conformation Attributed to Macromolecular Crowding. *J. Mol. Biol.* **2003**, *326*, 1227−1237.
(32) Winzor, D. J.; Wills, P. R. Molecular Crowding Effects of Linear Polymers in Protein Solutions. *Biophys. Chem.* **2006**, *119*, 186−195.

DOI: 10.1021/acs.jpcb.6b13076
J. Phys. Chem. B 2017, 121, 769−779

(33) Choi, J.; Muniyappan, S.; Wallis, J. T.; Royer, W. E.; Ihee, H. Protein Conformational Dynamics of Homodimeric Hemoglobin Revealed by Combined Time-Resolved Spectroscopic Probes. *ChemPhysChem* **2010**, *11*, 109−114.
(34) Choi, J.; Yang, C.; Kim, J.; Ihee, H. Protein Folding Dynamics of Cytochrome *c* Seen by Transient Grating and Transient Absorption Spectroscopies. *J. Phys. Chem. B* **2011**, *115*, 3127−3135.
(35) Yang, C.; Choi, J.; Ihee, H. The time Scale of the Quaternary Structural Changes in Hemoglobin Revealed Using the Transient Grating Technique. *Phys. Chem. Chem. Phys.* **2015**, *17*, 22571−22575.
(36) Harigai, M.; Imamoto, Y.; Kamikubo, H.; Yamazaki, Y.; Kataoka, M. Role of an N-terminal Loop in the Secondary Structural Change of Photoactive Yellow Protein. *Biochemistry* **2003**, *42*, 13893−13900.
(37) Tsierkezos, N. G.; Molinou, I. E. Thermodynamic Properties of Water Plus Ethylene Glycol at 283.15, 293.15, 303.15, and 313.15 K. *J. Chem. Eng. Data* **1998**, *43*, 989−993.
(38) Sun, T. F.; Teja, A. S. Density, Viscosity, and Thermal Conductivity of Aqueous Ethylene, Diethylene, and Triethylene Glycol Mixtures between 290 K and 450 K. *J. Chem. Eng. Data* **2003**, *48*, 198−202.
(39) Han, F.; Zhang, J. B.; Chen, G. H.; Wei, X. H. Density, Viscosity, and Excess Properties for Aqueous Poly(ethylene glycol) Solutions from 298.15 to 323.15 K. *J. Chem. Eng. Data* **2008**, *53*, 2598−2601.
(40) Gonzalez-tello, P.; Camacho, F.; Blazquez, G. Density and Viscosity of Concentrated Aqueous-Solutions of Polyethylene-Glycol. *J. Chem. Eng. Data* **1994**, *39*, 611−614.
(41) Arakawa, T.; Timasheff, S. N. Mechanism of Poly(ethylene glycol) Interaction with Proteins. *Biochemistry* **1985**, *24*, 6756−6762.
(42) Daillant, J. G. P.; Marques, C.; Muller, P.; Tran Tranh Van, J. *Short and Long Chains at Interfaces*; Editions Frontières: Gif-sur-Yvette, 1995; Vol. *30*.
(43) Erlkamp, M.; Grobelny, S.; Winter, R. Crowding Effects on the Temperature and Pressure Dependent Structure, Stability and Folding Kinetics of Staphylococcal Nuclease. *Phys. Chem. Chem. Phys.* **2014**, *16*, 5965−5976.
(44) Granath, K. A. Solution Properties of Branched Dextrans. *J. Colloid Sci.* **1958**, *13*, 308−328.
(45) Ihee, H.; Rajagopal, S.; Srajer, V.; Pahl, R.; Anderson, S.; Schmidt, M.; Schotte, F.; Anfinrud, P. A.; Wulff, M.; Moffat, K. Visualizing Reaction Pathways in Photoactive Yellow Protein from Nanoseconds to Seconds. *Proc. Natl. Acad. Sci. U.S.A.* **2005**, *102*, 7145−7150.
(46) Takeshita, K.; Imamoto, Y.; Kataoka, M.; Mihara, K.; Tokunaga, F.; Terazima, M. Structural Change of Site-Directed Mutants of PYP: New Dynamics during pR State. *Biophys. J.* **2002**, *83*, 1567−1577.
(47) Kaledhonkar, S. Structural Dynamics of Photoactive Yellow Protein. Ph.D. Thesis, Oklahoma State University, Stillwater, OK, 2013.
(48) Choi, J.; Terazima, M. Denaturation of a Protein Monitored by Diffusion Coefficients: Myoglobin. *J. Phys. Chem. B* **2002**, *106*, 6587−6593.
(49) Delaglio, F.; Grzesiek, S.; Vuister, G. W.; Zhu, G.; Pfeifer, J.; Bax, A. NMRPipe: A Multidimensional Spectral Processing System Based on UNIX Pipes. *J. Biomol. NMR* **1995**, *6*, 277−293.
(50) Goddard, T. D.; Kneller, D. G. *SPARKY 3*; University of California: Francisco.
(51) Pool, T. J.; Oktaviani, N. A.; Kamikubo, H.; Kataoka, M.; Mulder, F. A. ^{1}H, ^{13}C, and ^{15}N Resonance Assignment of Photoactive Yellow Protein. *Biomol. NMR Assignments* **2013**, *7*, 97−100.
(52) Borgstahl, G. E.; Williams, D. R.; Getzoff, E. D. 1.4 A Structure of Photoactive Yellow Protein, a Cytosolic Photoreceptor: Unusual Fold, Active Site, and Chromophore. *Biochemistry* **1995**, *34*, 6278−6287.
(53) Düx, P.; Rubinstenn, G.; Vuister, G. W.; Boelens, R.; Mulder, F. A.; Hard, K.; Hoff, W. D.; Kroon, A. R.; Crielaard, W.; Hellingwerf, K. J.; et al. Solution Structure and Backbone Dynamics of the Photoactive Yellow Protein. *Biochemistry* **1998**, *37*, 12689−12699.
(54) Petoukhov, M. V.; Franke, D.; Shkumatov, A. V.; Tria, G.; Kikhney, A. G.; Gajda, M.; Gorba, C.; Mertens, H. D.; Konarev, P. V.; Svergun, D. I. New Developments in the Program Package for Small-Angle Scattering Data Analysis. *J. Appl. Crystallogr.* **2012**, *45*, 342−350.

DOI: 10.1021/acs.jpcb.6b13076
J. Phys. Chem. B 2017, 121, 769−779